

Identifying meteorite droppers among the population of bright ‘sporadic’ bolides imaged by the Spanish Meteor Network during the spring of 2022

E. Peña-Asensio,^{1,2*} J. M. Trigo-Rodríguez,^{2,3} A. Rimola,¹ M. Corretgé-Gilart,⁴ and D. Koschny⁵

¹Departament de Química, Universitat Autònoma de Barcelona 08193 Bellaterra, Catalonia, Spain

²Institut de Ciències de l’Espai (ICE, CSIC), Campus UAB, C/ de Can Magrans s/n, 08193 Cerdanyola del Vallès, Catalonia, Spain

³Institut d’Estudis Espacials de Catalunya (IEEC), 08034 Barcelona, Catalonia, Spain

⁴Universitat Politècnica de Catalunya (UPC), Carrer de Jordi Girona, 31, 08034 Barcelona, Spain

⁵TU Munich, Boltzmannstrasse 15, 85748 Garching, Germany

Accepted XXX. Received YYY; in original form ZZZ

ABSTRACT

The extraordinary weather conditions available between February and March 2022 over Spain have allowed us to analyze the brightest fireballs recorded by the monitoring stations of the Spanish Meteor Network (SPMN). We study the atmospheric flight of 15 large meteoroids to determine if they are meteorite dropper events to prepare campaigns to search for freshly fallen extraterrestrial material. We investigate their origins in the Solar System and their dynamic association with parent bodies and meteoroid streams. Employing our Python pipeline *3D-FireTOC*, we reconstruct the atmospheric trajectory utilizing ground-based multi-station observations and compute the heliocentric orbit. In addition, we apply an ablation model to estimate the initial and terminal mass of each event. Using a dissimilarity criterion and propagating backward in time, we check the connection of these meteoroids with known complexes and near-Earth objects. We also calculate if the orbits are compatible with recent meteoroid ejections. We find that $\sim 27\%$ of these fireballs are dynamically associated with minor meteoroid streams and exhibit physical properties of cometary bodies, as well as one associated with a near-Earth asteroid. We identify two meteorite-producing events; however, the on-site search was unsuccessful. By considering that these fireballs are mostly produced by cm-sized rocks that might be the fragmentation product of much larger meteoroids, our findings emphasize the idea that the population of near-Earth objects is a source of near-term impact hazards, existing large Earth-colliding meteoroids in the known complexes.

Key words: meteorites, meteors, meteoroids – comets: general – minor planets, asteroids: general

1 INTRODUCTION

The interplanetary medium is composed of countless millimeter- and centimeter-sized objects called meteoroids, some of which eventually cross the path of our planet (Brown et al. 2002; Murad & Williams 2002; Trigo-Rodríguez 2022). These small bodies are fragments produced by the catastrophic disruption or collisions of comets, asteroids, or even impacts on planets (Chapman 2010; Tóth et al. 2011; Gritsevich et al. 2012; Trigo-Rodríguez et al. 2014). Due to tidal forces and sublimation by high temperatures of the Sun, cometary aggregates and rubble pile asteroids with efficient disruption processes suffer fragmentations in their passage through the perihelion, scattering meteoroids throughout their orbit that constitute the so-called meteoroid streams (also known as meteor showers) (Jenniskens 1994, 1998, 2006; Vaubaillon et al. 2019). Some of these meteoroid streams have Earth-intersecting orbits, so they are generally repeated in annual cycles. After experiencing different physical phenomena such as orbital perturbations, impacts with other objects, Yarkovsky, YORP, or Poynting-Robertson effect, other meteoroids suffer time scale decoherence and end up their space travel impacting on our planet as sporadic events, that is, apparently not associated with any known

complex (Olsson-Steel 1986; Bottke et al. 2000; Pauls & Gladman 2005; Brož 2006; Koschny et al. 2019).

The impact of these objects at high velocity with the upper part of our atmosphere produces a luminous phase in the visible range due to the collision with the atoms of the air and the consequent melting, evaporation, and progressive ionization of the meteoroid material (Ceplecha et al. 1998; Silber et al. 2018). This phenomenon is known as a meteor and is called a fireball or bolide if its magnitude is greater than that of Venus. From the observation and analysis of fireballs with ground-based multi-stations, more than 10 major showers have been established (Quadrantids, April Lyrids, η -Aquarids, Southern δ -Aquarids, Perseids, Orionids, Taurids, Leonids, Geminids and Ursids), that is, meteoroid streams that present activity of more than 10–15 meteors per hour (Bagnall 2021). However, there are hundreds of minor showers with lower activities as well as near-Earth asteroids, many of them poorly studied, that can produce bright fireballs and, therefore, potentially meteorite dropper events, just as being a source of impact hazard to the Earth (Voloshchuk & Kashcheev 1996; Halliday 1987; Madieto & Trigo-Rodríguez 2008; Borovička et al. 2015; Trigo-Rodríguez et al. 2017; Trigo-Rodríguez & Blum 2022; Peña-Asensio et al. 2022).

The months between January and April are especially relevant from the meteor science point of view as meteorite fall rates display a peak during the beginning of spring in either hemisphere (Halliday

* E-mail: eloy.pena@uab.cat, eloy.peas@gmail.com

Table 1. Location of the fireball observation points involved in this work.

Station	Name	Long (°)	Lat (°)	Alt (m)
A	Alpicat	0.5568	41.6676	252
B	Barx	-0.3041	39.0146	336
C	Benicàssim	0.0386	40.0342	15
D	Calar Alto	-2.549	37.2212	2152
E	Cebreros	-4.3693	40.4541	700
F	Corbera	1.8906	41.4092	501
G	Estepa	-4.8766	37.2914	537
H	GranTeCan	-17.8919	28.7567	2267
I	La Murta	-1.6756	38.0967	469
J	Monfragüe	-6.0108	39.7736	411
K	Morata de Jalón	-1.4821	41.474	415
L	Olocau	-0.5363	39.6744	225
M	Playa Blanca	-13.8241	28.8747	10
N	Puertollano	-4.1129	38.7032	697
O	Sant Mateu	0.1758	40.465	349

& Griffin 1982). Unfortunately, the weather during winter and spring is usually not helpful for fireball monitoring and clouds generally prevent detailed trajectory reconstruction and strewn-field estimates. In this sense, the months of February and March 2022 were especially clement in the Spanish territory so the Spanish Meteor Network (SPMN) has been able to record and analyze several spectacular fireballs, many of them associated with minor meteoroid streams rather than being sporadic.

In section 2, we first outline the SPMN network’s current infrastructure that has allowed recording these events with multiple stations. We also mention the methodology applied for fireball analysis. In section 3, we describe the results of the atmospheric flight reconstruction, terminal mass prediction, and heliocentric orbit calculation. In section 4, we analyze the dynamic associations with parent bodies, near-Earth asteroids and comets, and minor and major meteoroid streams. In addition, we examined the compatibility of these events being recently ejected meteoroids. Finally, we discuss the results in section 5 and offer our conclusions in section 6.

2 DATA COLLECTION AND METHODOLOGY

Since its creation in 2005, thanks to the operability of the SPMN network, the whole sky of continental Spain is monitored full time, the last decade also including the Balearic and Canary Islands. Currently, a total of 34 stations with charged-coupled device (CCD) video and all-sky cameras are operational, some of them equipped with spectrometers. In addition, three forward-scatter detectors monitor radio meteors (Trigo-Rodríguez et al. 2004). The stations involved in the events analyzed in this work are shown in Table 1, also incorporating the recently installed *AllSky7* camera at European Space Agency Cebreros’ station. This camera array allowed us to record 169 bright meteors up to an apparent magnitude of -6 between February and March of 2022, from which we selected the 15 largest multi-station bolides for analysis.

New video processing and trajectory calculation techniques allow the automation of the analysis process of meteors, bolides, and artificial fireballs produced by atmospheric re-entries of human-made objects. We developed the *3D-FireTOC* Python code that automates this study allowing the reconstruction of atmospheric trajectories and the calculation of heliocentric orbits from multiple recordings by using the intersection of planes method (Peña-Asensio et al. 2021b,a). Unlike traditional analytical methods, which solve the orbit by cor-

recting for zenith attraction and diurnal aberration (Ceplecha 1987), we have now implemented the accurate IAS15 high-order N-body integrator with an adaptive time step included in the REBOUND package to compute the heliocentric orbit (Rein & Spiegel 2015). The integrator is based on the RADAU-15 developed in Everhart (1985) and has a high performance resolving close encounters. We account for the Earth’s and Moon’s oblateness by including the J2 and J4 gravitational harmonic coefficients thanks to the REBOUNDx module (Tamayo et al. 2020).

For most cases, we performed the astrometric calibration by solving the polynomial modification of Borovička (1992) proposed by Bannister et al. (2013), which exhibits a better convergence while ensuring a very excellent level of uncertainty. To achieve the best fit, we use a simplicial homology global optimization algorithm to find the absolute minimum (Endres et al. 2018). For recordings with sufficient background stars, we apply the method proposed in Borovička et al. (1995), which produces even lower errors down to 0.01° for azimuth and elevation. All calibrations are also cross-checked with the quadratic model described in Peña-Asensio et al. (2021b).

With the mean uncertainties obtained in the astrometry for the camera calibration fit, we generate 1,000 clones to perform a Monte Carlo simulation following a Gaussian distribution applied to each detected point. We propagate every clone backward starting with its pre-atmospheric velocity from the beginning of the detected luminous phase until they are outside the Earth’s influence, specifically, at 10 times the Earth Hill sphere. We then integrate forward to the date of impact but without taking into account the gravitational attraction of the Earth-Moon system to obtain the osculating orbital elements at the time of the detection (referred to the J2000 equinox).

We further perform a backward integration over 10,000 years evaluating the evolution of an orbital dissimilarity criterion to test the dynamic association with parent body candidates. This is necessary as the most favorable candidate at the time of impact is not always the most reliable because it may be the result of a coincidence at that precise date. The meteoroid is integrated with its corresponding 1,000 clones generated from the uncertainties and the meteoroid streams are modeled by 18 equally spaced distributed particles over the true anomaly. Based on the orbital dissimilarity criterion, we assume that an association is robust enough if it remains below the cutoff for 5,000 years, minimizing the probability of being a random association (Porubčan et al. 2004).

Different techniques have been developed and discussed to establish the association between meteors and meteor showers or parent bodies, and they are still a source of debate today. One of the most established and widely used criteria is D_D (Drummond 1981), which is a semi-quantitative approach to measure the dissimilarity of two orbits as a function of their orbital parameters in the five-dimensional phase.

Based on the D_{SH} criterion (Southworth & Hawkins 1963), the D_D criterion was defined as:

$$D_D^2 = \left(\frac{e_B - e_A}{e_B + e_A} \right)^2 + \left(\frac{q_B - q_A}{q_B + q_A} \right)^2 + \left(\frac{I_{BA}}{\pi} \right)^2 + \left(\frac{e_B + e_A}{2} \right)^2 \left(\frac{\theta_{BA}}{\pi} \right)^2, \quad (1)$$

where e is the eccentricity, q is the perihelion distance, I_{BA} is the angle between the orbital planes, π_{BA} is the difference between longitudes of perihelia measured from the intersection of both orbits, and θ_{BA} is the orbit angle between the lines of apsides.

The thresholds of the dissimilarity functions, far from defining an exact barrier, offer an approximation with fair statistical significance,

which, in addition, may vary depending on the inclination of the orbits and the population size. Therefore, they are not a defining indicator, and it is also necessary to verify that the orbits are not only similar at a given time but also that this similarity lasts over time. In this sense, we use 0.18 as a cut-off for D_D (Galligan 2001). Although this threshold value is high, we use it as a first filter, but not as the only association condition as we also check its evolution over time.

In addition, we evaluate if the separation of the meteoroid from its possible parent body could have occurred in relatively short timescales. For this purpose, during the orbital integration, we monitor the minimum distance between the objects and the change in the velocity vector that would be needed to move from one orbit to the other one. In this way, we can observe if the velocity change is compatible with typical collisional ejection processes between small bodies.

We also examined Tisserand's parameter with respect to Jupiter T_j , which is helpful to determine the evolution of small bodies since it remains broadly constant for long periods. It is used to classify planet-crossing objects, usually, as Jupiter-family comets (JFCs) if $2 < T_j < 3$ and asteroidal when $T_j > 3$.

We evaluate the catastrophic disruption for each event by obtaining the ram pressure at peak brightness, that is, the bulk aerodynamic strength ($s = \rho \cdot v^2$) accordingly to the U.S. standard atmosphere 1976 (Bronshten 1981). This parameter is typically used to mechanically characterize the meteoroid and to classify the material regarding the bulk density. For events that do not present an explosion, we evaluate the peak of maximum brightness, thus obtaining only an estimate of the lower limit for the composition.

Additionally, assuming an isothermal atmosphere and applying the dynamic third-order time-dependent system for characterizing meteor deceleration based on the velocity (v) and the height (h), we compute the ballistic coefficient (α) and mass loss parameter (β) (Gritsevich & Stulov 2006; Gritsevich 2008, 2009; Gritsevich et al. 2012; Turchak & Gritsevich 2014):

$$F_i(h_i, v_i, \alpha, \beta) = 2\alpha e^{-h_i} - \Delta_i e^{-\beta}, \quad (2)$$

with $\Delta_i = \overline{Ei}(\beta) - \overline{Ei}(\beta v_i^2)$, $i = 1, 2, \dots, n$, where

$$\overline{Ei}(x) = \int_{-\infty}^x \frac{e^t dt}{t} dx.$$

These adimensional parameters are defined as

$$\alpha = \frac{1}{2} c_d \frac{\rho_0 h_0 S_0}{M_0 \sin \gamma}, \quad (3)$$

and

$$\beta = (1 - \mu) \frac{c_h v_0^2}{2 c_d H^*}, \quad (4)$$

where c_d is the drag coefficient, ρ_0 is the atmospheric density at sea level, h_0 is the scale height for a homogeneous atmosphere and γ is the slope of the fireball to the local horizon, M_0 is the meteoroid mass before impacting the top of the atmosphere, μ is the dimensionless shape change parameter, c_h is the heat transfer coefficient, v_0 is the entry velocity, and H^* is the sublimation heat. μ is a constant value that relates the cross-sectional area S with the mass as follows: $S/S_0 = (M/M_0)^\mu$ (Lyytinen & Gritsevich 2016). Note that as it is an atmospheric flight dynamics model with an asymptotic solution, the minimization problem itself yields an initial velocity at infinity that corresponds to the pre-atmospheric velocity.

These parameters allow properly describing the atmospheric flight

and estimating the meteor fate based on the so-called $\alpha - \beta$ criterion (Sansom et al. 2019). The boundaries that delimit the fall likelihood (with a terminal mass threshold of 50 g) are determined by the two extreme values of the shape change coefficient: $\mu = 0$ when the meteoroid is not spinning and $\mu = 2/3$ when the meteoroid surface is equally ablated due to the rotation.

From the aerodynamic strength values, we assign a meteoroid bulk density based on Chyba et al. (1993): cometary if $s < 10^5 Pa$; carbonaceous if $10^5 Pa < s < 10^6 Pa$; rocky if $10^6 Pa < s < 10^7 Pa$; and rocky-iron if its aerodynamic strength is greater than $10^7 Pa$. This allows us to fit the object size D , the pre-atmospheric mass M_0 , and the terminal mass M_t (the final mass at the end of the luminous atmospheric phase), being

$$M_0 = \left(\frac{1}{2} \frac{c_d A_0 \rho_0 h_0}{\alpha \rho_m^{2/3} \sin \gamma} \right)^3, \quad (5)$$

where A_0 is the pre-atmospheric shape coefficient.

The terminal mass can be computed using the last observed velocity in the following instant mass equation

$$M(t) = M_0 e^{-\frac{\beta}{1-\mu} \left(1 - \left(\frac{v(t)}{v_0} \right)^2 \right)}, \quad (6)$$

where $v(t)$ is the instantaneous velocity.

3 ATMOSPHERIC FLIGHT AND HELIOCENTRIC ORBIT

Once the most suitable recordings of each event have been selected, and the lenses of each camera have been calibrated to correct distortions and found the transformation between pixel and position in the sky, we can apply the triangulation using the weighted method of the intersection of planes for multiple stations to obtain the real position of the meteoroid in each frame. Each station recorded the events in a single shot, except for the grazing meteoroid SPMN080322, which moved out of the field of view. Therefore, we had to combine the recordings from two cameras to obtain the complete luminous trail. Figure 1 shows a composite of overlapping images of some of the events recorded and analyzed in the following section.

In some images, like the one of the SPMN060222 fireball captured in color from Corbera, an intense reddish tone due to the glowing ionized air can be seen, although further color calibrations are necessary for a precise determination of the tone. In the trace drawn during the atmospheric flights, it can be seen how several of them show multiple brightness peaks, as a result of the rapid rotation and differentiated ablation, while others only exhibited a large final flare due to the catastrophic disruption. The beginning and ending position, distance flight, and direction of the luminous phase for each event are shown in Table 2. The initial heights range from ~ 120 to 83 km and terminal heights (before starting the dark flight) range from ~ 80 to 13 km. As expected, the azimuth and slope have a random distribution, with the average slope being around 45° . Note that the slope is measured with respect to the local horizon, 0° corresponding to a fully grazing meteor. In this regard, we see how the event SPMN010322A traveled through the atmosphere a notably greater distance than the rest (~ 198 km), its slope being close to 10° . Event SPMN080322A, although also with a shallow slope, underwent a rapid disruption at 70 km altitude, which did not allow it to cover a long distance.

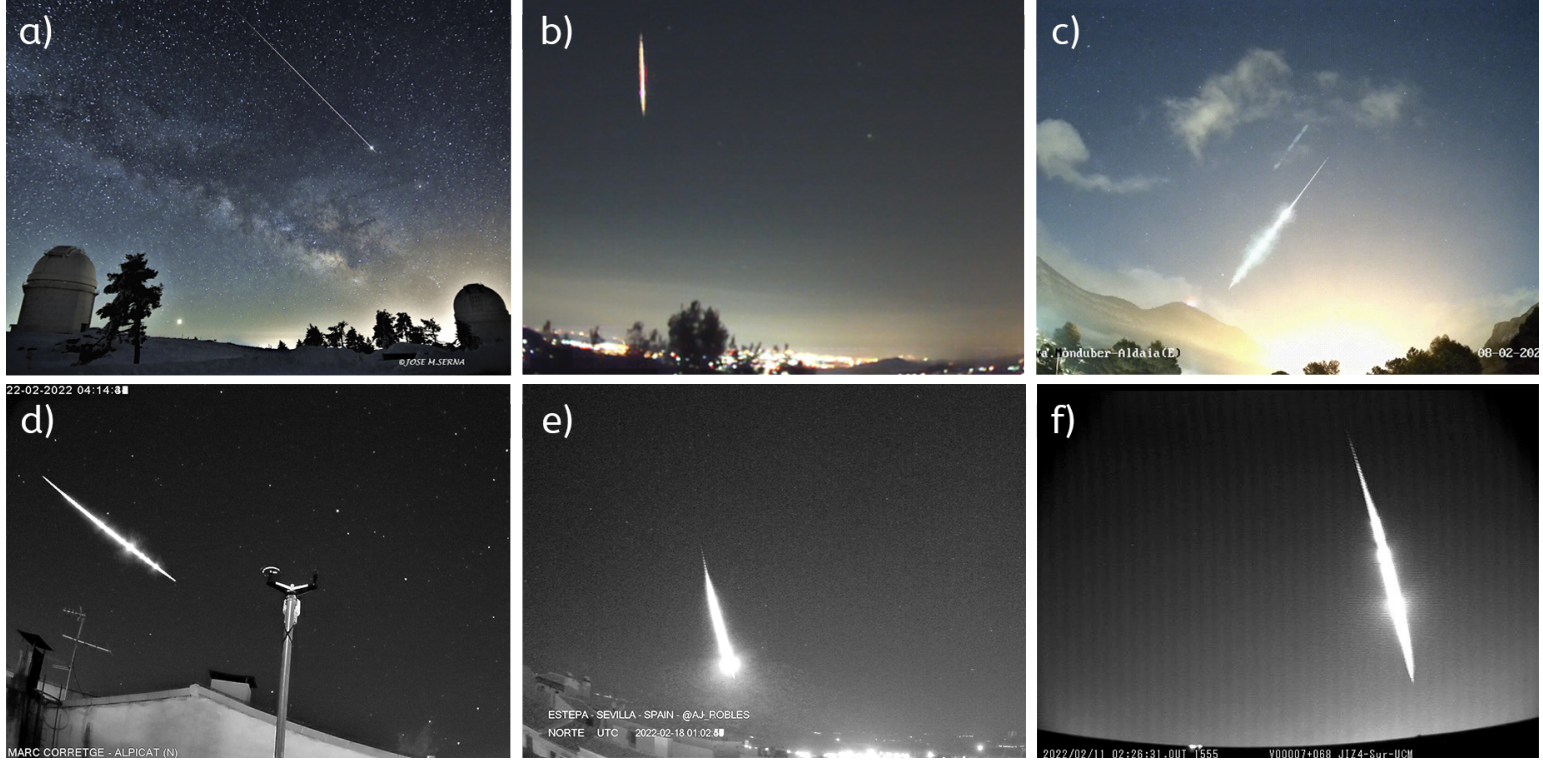


Figure 1. Selection of blended frames of some of the events analyzed in this work: a) SPMN090322C from Calar Alto by José M. Serna García, b) SPMN060222 from Corbera, c) SPMN080222B from Barx, d) SPMN220222 from Alpicat, e) SPMN180222 from Estepa, and f) SPMN110222 from Madrid.

Table 2. Recorded fireballs with the beginning and ending position, flight distance traveled, and direction of the atmospheric flight.

SPMN code	Datetime (UTC)	Stations	Long ₀ (°)	Lat ₀ (°)	h ₀ (km)	Long _f (°)	Lat _f (°)	h _f (km)	Distance (km)	Azimuth (°)	Slope (°)
060222	2022-02-06 23:03:20	A,F	4.324±0.011	42.848±0.004	91.3±0.4	4.392±0.009	42.8570±0.0031	69.16±0.26	22.9±0.5	80±5	75±4
080222A	2022-02-08 01:09:54	A,B,K	-2.5529±0.0029	41.2470±0.0012	101.594±0.028	-2.5542±0.0029	41.6429±0.0014	41.06±0.08	77.54±0.32	359.4±0.5	51.33±0.11
080222B	2022-02-08 23:31:00	A,B	1.1353±0.0010	38.9446±0.0008	89.16±0.07	1.1055±0.0009	39.1885±0.0007	36.134±0.024	60.68±0.22	353.97±0.32	60.940±0.032
110222	2022-02-11 02:26:30	B,E,O	-3.625±0.009	39.702±0.007	89.8±0.8	-3.731±0.005	39.455±0.006	37.50±0.21	65.5±0.5	198.7±2.8	52.9±1.2
140222B	2022-02-14 20:59:07	G,I,N	-3.5864±0.0014	37.8739±0.0004	94.646±0.025	-3.2628±0.0009	37.78175±0.00030	49.547±0.018	60.51±0.22	109.69±0.05	48.18±0.06
180222	2022-02-18 01:02:45	I,J,O	-6.1642±0.0023	39.380±0.004	88.79±0.06	-6.0776±0.0034	39.5080±0.0034	12.87±0.15	82.9±0.8	26.8±1.3	66.43±0.18
220222	2022-02-22 04:34:24	A,K	-0.5435±0.0010	42.3780±0.0005	83.77±0.08	0.1736±0.0004	42.2556±0.0005	38.92±0.04	80.57±0.13	102.42±0.08	33.814±0.015
010322A	2022-03-01 00:48:01	A,C,L	2.6121±0.0034	41.3954±0.0020	95.79±0.07	1.4258±0.0018	39.9335±0.0015	50.499±0.024	197.0±0.4	211.99±0.07	13.293±0.024
010322B	2022-03-01 01:43:57	B,O	-2.793±0.008	39.9817±0.0019	101.07±0.30	-3.258±0.010	39.5159±0.0019	71.70±0.24	74.2±0.7	217.7±1.0	23.3±0.5
080322A	2022-03-08 00:36:59	A,F	0.8633±0.0008	40.6421±0.0005	96.82±0.08	1.7423±0.0006	41.00590±0.00030	80.13±0.05	87.00±0.12	60.904±0.032	11.06±0.06
080322B	2022-03-08 19:26:22	A,L	1.8383±0.0005	40.4211±0.0005	83.58±0.05	1.8210±0.0005	40.4374±0.0005	36.786±0.021	57.70±0.18	320.613±0.024	54.09±0.10
090322B	2022-03-09 03:01:46	A,B,C	-1.5107±0.0010	39.8088±0.0004	120.65±0.07	-2.0243±0.0011	39.94857±0.00035	77.071±0.035	71.19±0.13	289.42±0.04	37.75±0.12
090322C	2022-03-09 04:25:38	D,I	-2.0192±0.0007	36.9452±0.0009	92.94±0.15	-2.1597±0.0006	36.4849±0.0017	58.54±0.10	64.80±0.05	193.73±0.15	32.07±0.23
100322	2022-03-10 01:38:19	H,M	-15.540±0.014	30.0550±0.0034	85.4±0.8	-15.600±0.022	29.689±0.005	29.2±0.6	82.5±0.6	188±5	42.94±0.17
120322	2022-03-12 22:15:53	A,L	1.1473±0.0004	40.7151±0.0007	94.21±0.09	1.09818±0.00035	40.7597±0.0006	67.85±0.05	27.40±0.16	319.4±0.4	74.30±0.25

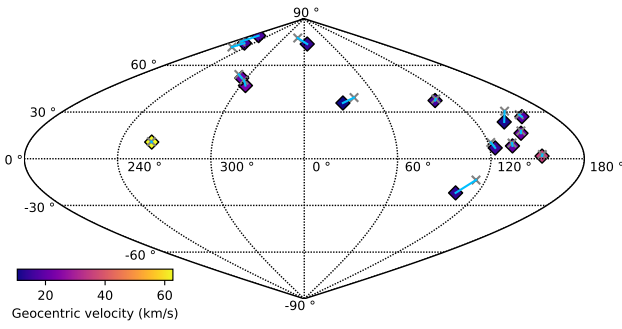


Figure 2. Sinusoidal projection of the geocentric (diamond) and apparent (gray cross) radiant pairs. Radiant pairs are connected with a light blue line. Geocentric radiants are color-coded according to their geocentric velocity.

Using the height at which the brightest flare occurs, the air density, and the velocity at that point, we calculate the aerodynamic strength. According to the value of this dynamic pressure, we estimate the bulk density as explained in Section 2, which is used to calculate the pre-atmospheric diameter assuming a perfect sphere. To obtain the ballistic coefficient and the mass loss parameter, we assume an aerodynamic drag coefficient of 1.3 and a shape change coefficient of 2/3 (Gritsevich & Koschny 2011). The geocentric velocities range from ~ 63 to 11 km/s, and most of the radiant pairs are in the northern hemisphere, as depicted in Figure 2 in sinusoidal projection. All the computed parameters are shown in Table 3 and 4.

Two meteoroids penetrate up to ~ 30 and 13 km altitude starting the dark flight at a velocity of ~ 8 and 20 km/s, respectively. As can be seen in Figure 3, from the application of the $\alpha - \beta$ criterion and assuming 50 g as the minimum terminal mass to produce a recoverable fall, event SPMN100322 had some possibility of generating a meteorite with a mass of ~ 140 g, and event SPMN180222 was likely to be a ~ 430 g meteorite dropper. Unfortunately, a field search campaign was prepared but no fragments were recovered.

The computed osculating orbital elements at the time of impact of the analyzed fireballs are compiled in Table 5. As an example of the Monte Carlo simulation, Figure 4 shows a heat map of the semi-major axis and inclination distribution for the 1,000 clones of event SPMN010322A at the time of impact ($t=0$ year without Earth-Moon gravitational focusing correction) and at the end of the backward orbital integration ($t=-10,000$ year).

Four orbits present very high eccentricity values with large semi-major axes, five can be classified as Jupiter-family comets, while four are asteroid-like orbits. As expected, the orbits tend to be of low inclination, with the exception of SPMN090322B which has an inclination of 122° . None of the meteoroids had close encounters with the Moon prior to the impact.

4 DYNAMIC ASSOCIATION WITH METEOROID STREAMS AND PARENT BODIES

The study of the associations of meteoroids that impact our planet with parent bodies or meteoroid streams is not a trivial task. There

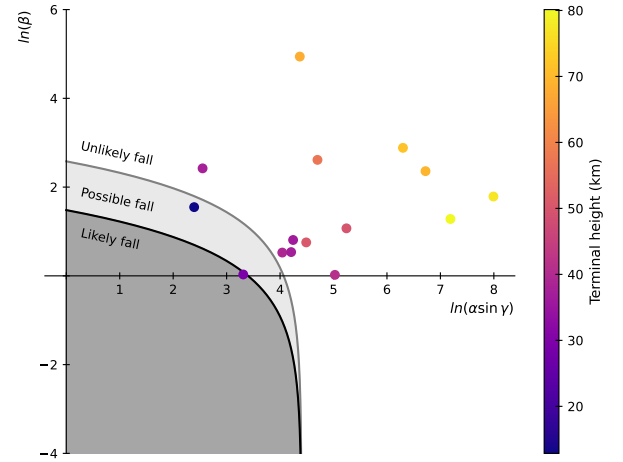


Figure 3. Distribution of the 15 fireballs analyzed over the Spanish territory during February and March 2022 according to the $\alpha - \beta$ criterion. The color bar shows the terminal height, the gray solid curve the boundary for a 50 g meteorite assuming no spin of the meteoroid, and the black solid curve the boundary for a 50 g meteorite assuming equal ablation over the entire meteoroid surface. We assume $\mu = 2/3$ for all meteoroids.

are numerous mechanisms that prevent the correct linking of meteors with their origins, from the intrinsically chaotic behavior of planetary systems to non-gravitational effects and sporadic collisions and interactions (Trigo-Rodríguez et al. 2005). Because of the high probability that two orbits are randomly associated (Wiegert & Brown 2004), we have not only analyzed the similarity of the orbits at the time of impact but also studied their robustness over time. From the time evolution of the parent body dissimilarity criterion, we found some dynamic associations. Figure 5 shows the evolution of the dissimilarity criterion during the orbital integration of the 15 events analyzed in this work, along with their most favorable parent body candidates or meteor shower. Table 6 shows each event with its most likely association, along with the years of time it lasts under the D_D threshold, the minimum encounter distance, the required ejection velocity at the time of minimum distance, and the minimum required ejection velocity.

5 out of 15 events, that is, about 30% of the bright fireballs, are below the cut-off for at least 5,000 years. 4 events would be associated with minor showers ($\sim 27\%$) and 1 fireball associated with a near-Earth asteroid ($\sim 7\%$). In all the associated cases, the required ejection velocity needed to transform the parent orbit into the meteoroid orbit is in good agreement with the estimated range for collisions between objects, which can produce a kick of a few kilometers per second (Melosh 1984).

5 DISCUSSION

In relation to the various ablation behaviors observed, it is important to note that this could be the result of the differences between chondritic meteoroid and cometary aggregate bulk properties. The low density and high porosity of the latter are directly related to their aerodynamic strengths (Blum et al. 2006). Cometary streams typically produce centimeter-sized projectiles causing fireballs with disruptive flares, and multiple sudden brightness increases or a catastrophic final flare. Due to the heterogeneity of the meteoroid components, the evaporation temperature of each one is reached at different

Table 3. Recorded fireballs with aerodynamic strength, ballistic coefficient, mass loss parameter, pre-atmospheric diameter, pre-atmospheric mass, and terminal mass.

SPMN code	s (kPa)	α	β	D (cm)	M_0 (g)	M_t (g)
060222	18.9±0.4	$(8.6\pm0.7)\cdot10^2$	10.6±1.0	1.17±0.08	0.83±0.16	<1
080222A	724±7	195.1±3.4	1.023±0.031	6.35±0.10	134±7	11.3±0.5
080222B	501.06±0.25	79.72±0.27	2.244±0.004	13.90±0.04	1405±13	5.363±0.025
110222	361.6±3.5	16.1±1.9	11.3±1.7	76±8	$(2.3\pm0.7)\cdot10^5$	<1
140222B	78.16±0.15	253.7±1.5	2.917±0.017	5.121±0.027	70.3±1.1	<1
180222	1107±21	11.94±0.23	4.70±0.07	25.3±0.5	$(2.96\pm0.16)\cdot10^4$	432±34
220222	283.6±1.8	102.2±0.6	1.690±0.022	17.02±0.10	$(2.58\pm0.05)\cdot10^3$	33.9±1.2
010322A	209.4±1.1	387±6	2.13±0.04	10.87±0.16	673±29	2.93±0.17
010322B	17.17±0.33	$(1.38\pm0.28)\cdot10^3$	18±4	1.8±0.4	3.1±1.8	<1
080322A	2.935±0.019	6898±28	3.60±0.07	0.732±0.006	0.205±0.005	<1
080322B	364.7±2.2	82.9±0.8	1.709±0.026	14.42±0.16	$(1.57\pm0.05)\cdot10^3$	25.3±0.8
090322B	25.45±0.10	4831±29	5.974±0.015	0.3274±0.0013	0.01838±0.00022	<1
090322C	$(4.185\pm0.017)\cdot10^5$	255±4	9.11±0.17	7.16±0.08	192±7	106±20
100322	$(1.30\pm0.14)\cdot10^3$	40.3±3.4	1.03±0.33	10.1±0.8	$(1.9\pm0.5)\cdot10^3$	$(1.4\pm0.8)\cdot10^2$
120322	19.55±0.26	82±22	140±34	12±4	$(1.0\pm1.1)\cdot10^3$	<1

Table 4. Recorded fireballs with right ascension and declination of the radiant, apparent, geocentric, and heliocentric velocities.

SPMN code	RA_a (°)	Dec_a (°)	RA_g (°)	Dec_g (°)	RA_h (°)	Dec_h (°)	$V_{a,0}$ (km/s)	$V_{a,t}$ (km/s)	V_g (km/s)	V_h (km/s)
060222	108±4	38.4±2.2	106±4	37.4±2.5	65.6±0.9	5.8±1.0	19.61±0.09	11.229±0.033	16.32±0.09	41.5±0.5
080222A	153.14±0.33	2.69±0.11	152.86±0.34	1.70±0.12	106.92±0.06	-7.911±0.031	37.17±0.24	16.329±0.029	35.46±0.25	39.91±0.33
080222B	135.60±0.15	10.09±0.04	135.18±0.16	8.23±0.05	82.10±0.05	-4.635±0.004	23.475±0.005	9.7592±0.0022	20.666±0.006	37.79±0.04
110222	211.58±0.34	71.8±2.0	217.9±1.1	74.3±2.3	60.9±0.8	27.0±1.7	20.1±0.4	15.89±0.20	16.8±0.4	35.24±0.31
140222B	41.35±0.08	39.312±0.028	30.63±0.09	35.822±0.023	51.850±0.018	5.641±0.017	15.068±0.013	8.905±0.004	10.536±0.020	39.904±0.019
180222	146.3±0.5	17.90±0.28	145.2±0.5	16.39±0.29	91.44±0.10	1.29±0.07	23.95±0.08	20.045±0.013	21.32±0.09	38.79±0.23
220222	149.508±0.030	30.58±0.06	140.248±0.028	23.63±0.11	80.31±0.07	2.559±0.022	15.60±0.04	5.9502±0.0031	11.41±0.06	35.225±0.034
010322A	299.19±0.11	50.410±0.029	304.55±0.12	47.034±0.012	49.777±0.031	34.32±0.04	25.56±0.05	9.799±0.015	22.97±0.05	36.477±0.009
010322B	288.24±0.33	54.1±1.1	295.0±0.4	51.9±1.1	56.2±0.5	35±4	23.83±0.06	19.43±0.13	21.01±0.07	34.99±0.34
080322A	113.58±0.07	-13.672±0.026	104.83±0.12	-21.95±0.07	83.91±0.06	-13.79±0.07	17.157±0.030	13.560±0.006	13.40±0.04	39.542±0.029
080322B	121.84±0.05	10.43±0.09	123.60±0.04	6.96±0.07	91.87±0.07	-4.541±0.026	18.72±0.06	8.266±0.013	14.90±0.08	41.49±0.06
090322B	259.88±0.09	10.98±0.09	260.24±0.09	10.72±0.09	259.93±0.27	57.545±0.015	63.937±0.007	40.138±0.033	62.749±0.008	41.32±0.04
090322C	340.5±1.2	77.58±0.05	6.2±0.9	73.90±0.14	73.418±0.026	18.82±0.17	18.159±0.018	17.96±0.07	14.397±0.024	38.81±0.05
100322	200±12	75.3±1.7	205±17	79.1±1.8	84.42±0.31	24.54±0.33	20.2±0.7	8.358±0.030	17.0±0.9	38.3±1.4
120322	156.87±0.09	28.29±0.26	157.00±0.10	27.05±0.26	104.92±0.23	7±34	21.39±0.15	14.27±0.06	18.27±0.18	40.48±0.09

Table 5. Recorded fireballs with semi-major axis, eccentricity, inclination, perihelion distance, argument of the perihelion, ascending node, and Tisserand parameter (referred to the J2000 equinox). Uncertainty for the ascending node is 0.0001°.

SPMN code	a (au)	e	i (°)	q (au)	ω (°)	Ω (°)	T_j
060222	11±5	0.92±0.04	6.1±1.4	0.892±0.011	216.823±0.011	317.8516	1.60±0.21
080222A	4.3±0.6	0.938±0.007	14.69±0.10	0.2658±0.0030	120.6728±0.0030	138.9337	1.77±0.14
080222B	2.395±0.018	0.7285±0.0015	5.47±0.05	0.6504±0.0015	78.9636±0.0015	139.8736	3.015±0.014
110222	1.60±0.06	0.403±0.020	27.2±1.0	0.954±0.006	208.156±0.006	322.0380	4.02±0.11
140222B	4.344±0.033	0.7739±0.0017	5.655±0.010	0.98217±0.00005	170.87497±0.00005	325.8715	2.320±0.008
180222	3.05±0.18	0.783±0.011	1.53±0.13	0.662±0.005	255.517±0.005	329.0900	2.60±0.09
220222	1.605±0.007	0.4698±0.0026	2.68±0.05	0.8510±0.0005	235.6854±0.0005	333.2960	4.089±0.013
010322A	1.9276±0.0027	0.5469±0.0006	36.06±0.10	0.87346±0.00008	131.68867±0.00008	340.1080	3.413±0.004
010322B	1.57±0.06	0.411±0.020	35.36±0.14	0.922±0.007	139.445±0.007	340.1481	4.00±0.12
080322A	3.96±0.04	0.7532±0.0026	13.885±0.012	0.97727±0.00023	15.37103±0.00023	167.1195	2.392±0.012
080322B	13.5±1.0	0.931±0.005	4.68±0.04	0.9330±0.0004	28.9213±0.0004	167.8948	1.570±0.025
090322B	11.2±0.5	0.911±0.004	122.44±0.13	0.99250±0.00009	178.06764±0.00009	348.2148	1.108±0.020
090322C	3.16±0.04	0.688±0.004	18.90±0.07	0.98494±0.00007	168.69848±0.00007	348.2915	2.665±0.019
100322	2.8±0.9	0.65±0.12	24.60±0.17	0.98426±0.00012	192.22661±0.00012	349.1653	2.8±0.6
120322	6.05±0.30	0.862±0.008	7.92±0.04	0.8339±0.0023	229.2663±0.0023	352.0240	1.93±0.04

altitudes, giving rise to the so-called differential ablation (Gómez Martín et al. 2017). The aerodynamic overpressure experienced by meteoroids when they fragment allows for estimating their aerodynamic strength. This, in turn, allows for deducing the bulk properties of their meteoroid stream (Kresak 1982; Trigo-Rodríguez & Llorca

2006). These types of large fireballs associated with cometary vestiges are the result of rapid disruption in micrometric grains and the sudden ablation of volatile mineral phases driven by the thermal wave in the meteoroid head (Trigo-Rodríguez et al. 2019).

Even in such circumstances, it is remarkable that the sporadic con-

Table 6. Most likely parent body and meteoroid stream candidates for each event with the minimum D_D value, the years that fulfill the D_D criterion threshold, the minimum encounter distance, the required ejection velocity at the time of minimum distance, and the minimum required ejection velocity during the orbital integration.

SPMN code	Association	D_{min}	t_D (y)	S_{min} (au)	$V_{S,min}$ (km/s)	V_{min} (km/s)
060222	ρ Geminids	0.176	180	0.186	4.7	4.7
080222A	α Leonids	0.174	90	0.231	4.6	0.9
080222B	Southern δ Leonids	0.018	8720	0.129	0.8	0.4
110222	ω Cassiopeiids	0.101	10000	0.087	9.6	1.4
140222B	March Cassiopeiids	0.121	1610	0.145	10.2	0.5
180222	Southern δ Leonids	0.07	240	0.278	13.2	2.0
220222	Northern α Leonids	0.09	10000	0.05	5.8	1.4
010322A	2019 CV2	0.099	2640	0.264	6.0	1.7
010322B	2017 FM91	0.092	9990	0.104	6.6	2.3
080322A	2007 DZ40	0.073	800	0.144	3.1	1.1
080322B	February Hydrids	0.168	600	0.37	15.9	3.0
090322B	72 Ophiuchids	0.136	9990	0.811	14.3	0.4
090322C	March Cassiopeiids	0.084	110	0.34	10.9	0.8
100322	ψ Draconids	0.106	2080	0.37	5.1	2.0
120322	λ Leonids	0.125	1300	0.083	7.4	2.4

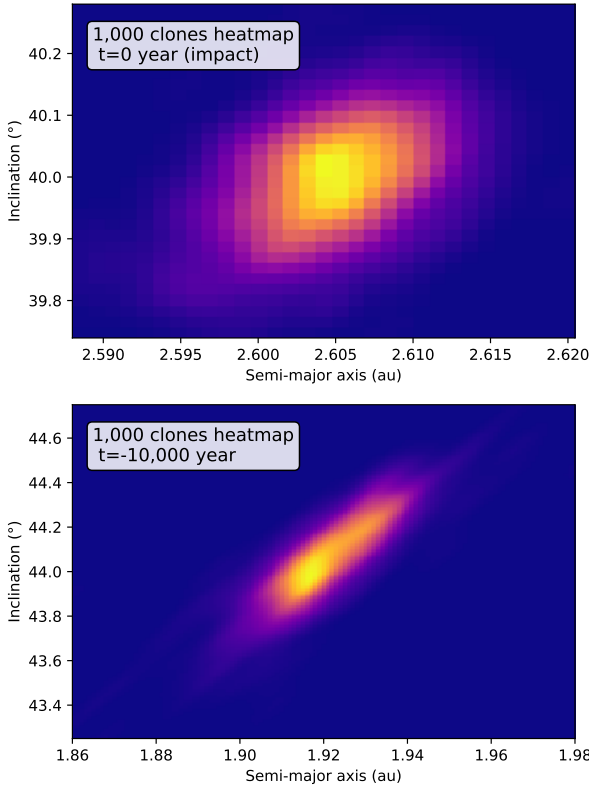


Figure 4. Typical heatmap of the inclination and semi-major axis distribution of the 1,000 clones for the SPMN010322A in the Monte Carlo simulation. The top figure corresponds to the time of impact ($t=0$ year) without Earth-Moon gravitational focusing correction. The bottom figure corresponds to the end of the backward orbital integration ($t=-10,000$ years).

tribution is not dominant at all. We found a very significant percentage of bright fireballs dynamically associated with minor showers. Although during the orbital integration there are no very close encounters despite the reasonable ejection velocities, we must point out that we have propagated 18 particles distributed in true anomaly throughout the orbit of the meteoroid streams, but at their nominal values for the rest of the orbital elements. Due to the orbital perturbations accumulated over time and their violent origin, either by tidal forces disruption or catastrophic collisions, the meteoroid streams spread toroidally along their orbit and gradually disperse. Some regions even undergo more pronounced decoherence than others due to the gravitational influence of the Earth-Moon system or nearby planets.

The minimum ejection velocities calculated to produce the meteoroid orbit from the parent body have a standard deviation range between 0.16 and 1.4 km/s (with an average standard deviation of 0.4 km/s) for the studied events. Although the ejection velocities found are compatible with collisions of small objects in the inner Solar System, this does not necessarily mean that these meteoroids have separated from their meteoroid stream or parent body recently; we just note it as a feasible possibility due to the usual disruption behavior of crumbling asteroids and comets.

Although remarkable, the high number of minor showers producing fireballs should not come as a surprise as such a percentage of meteors associated with meteoroid streams is not unusual. For example, percentages up to 80% between November and January were already reported belonging to meteor showers (Rao & Murthy 1974). On the other hand, among the 2,401 records studied by Lindblad (1971), apparently, 37% were associated with meteoroid streams. A similar percentage (41%) was found by Southworth & Hawkins (1963). Of the orbits analyzed by Jacchia & Whipple (1961), 65% were linked to a meteor shower. Regarding the Meteorite Observation and Recovery Project (MORP) database, 37% of the fireballs could be associated with meteoroid stream (Halliday et al. 1996). Terentjeva (1990) performed a grouping according to event candidates to produce meteorites, finding that 68% of 554 fireballs studied could be part of a shower. And also in good agreement with the results of this work, Babadjanov (1963) reported that of the 185 meteors studied, 73% appeared to be of cometary origin. Recent studies also show large percentages of meteors associated with meteor showers, for example,

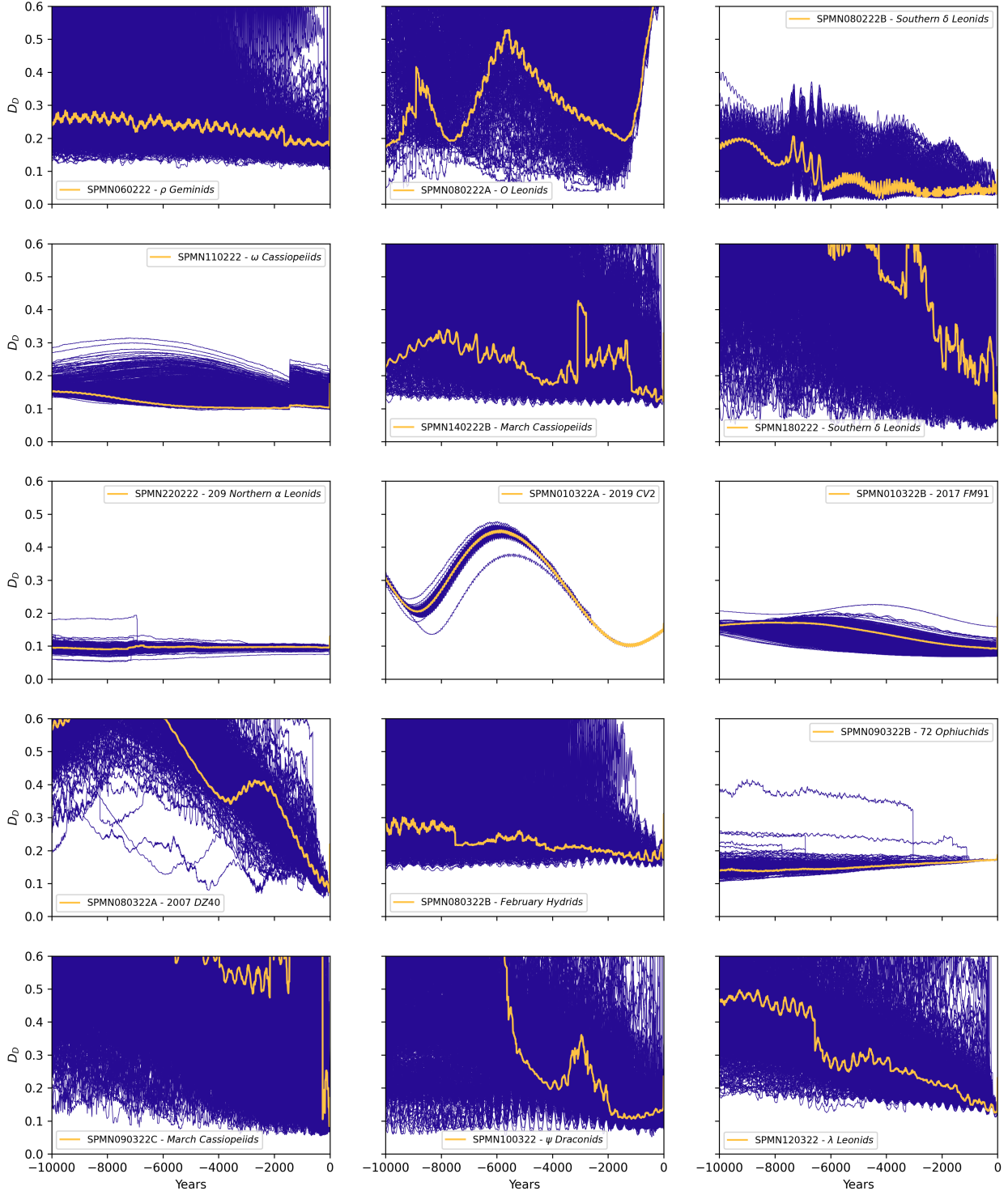


Figure 5. Evolution of the dissimilarity function D_D of the 15 meteoroids with their most favorable candidates during the orbital backward integration over 10,000. The 1,000 clones of each event are also shown.

45% in Colas et al. (2020) and 35% in Drolshagen et al. (2021). Regarding superbolides detected from space, 23% could be associated with meteoroid streams or near-Earth objects (Peña-Asensio et al. 2022).

Therefore, as previously studied, it is reasonable to expect that a large percentage of the meteors belong to minor meteoroid streams, but also, as we show in this work, some meteor showers can be a significant source of large projectiles for the Earth and the Moon.

6 CONCLUSION

The extraordinary meteorological conditions in Spain during the spring of 2022 have made it possible to obtain high-quality data related to the fireball activity produced, to a large extent, by minor meteoroid streams. Ground-based multi-station recordings were possible thanks to the ever-increasing atmospheric volume monitored by the SPMN network throughout Spain. We reported 15 bright bolides in February and March, two of them being potential meteorite dropper events. By applying novel computer vision techniques and improved methods of trajectory reconstruction and heliocentric orbit calculation implemented in our software *3D-FireTOC*, we have been able to study in detail the atmospheric flight and dynamic association of large cometary and asteroidal projectiles impacting our planet. Based on the trajectory data, we computed the initial and terminal mass, the aerodynamic strength, and the bulk density by means of an ablation model. In consequence, we claim that:

- Among the 169 bright meteors recorded during the spring of 2022 in Spain, 2 of them were potentially meteorite dropper events.
- We identify the minor showers of Leonids, Southern δ Leonids, ω Cassiopeids, Northern α Leonids, and 72 Ophiuchids, and the asteroid 2017 FM91 as sources of large projectiles during February and March.
- Nearby meteoroid streams can be efficient producers of large projectiles as they account for the $\sim 27\%$ of the fireballs.
- Near-Earth objects may be a greater source of impact risk than previously thought.
- It is needed to extend the study and cataloguing of minor showers, since, although they are not very active in terms of the number of meteors, our work indicates that they also produce large bolides annually.
- These findings support the idea that certain meteoroid streams associated with comets or asteroids may represent a short-term impact hazard.

Finally, we think that understanding the origin and mechanisms by which large meteoroids reach the Earth is of great scientific interest due to the possibility of associating complexes and parent bodies with fireballs and, ultimately, meteorites found on Earth and the Moon. The relevance of associations also reverts in outreach, as we can quickly inform the public about the origin of the fireballs reported by eyewitnesses.

ACKNOWLEDGEMENTS

This project has received funding from the European Research Council (ERC) under the European Union's Horizon 2020 research and innovation programme (grant agreement No. 865657) for the project “Quantum Chemistry on Interstellar Grains” (QUANTUMGRAIN). JMT-R and E.P.-A. acknowledge financial support from project PID2021-128062NB-I00 funded by

MCIN/AEI/10.13039/501100011033. AR acknowledges financial support from the FEDER/Ministerio de Ciencia e Innovación – Agencia Estatal de Investigación (PID2021-126427NB-I00, PI: AR). AR is indebted to DIUE (project 2017SGR1323), Cebreros #AMS81 ESA Ground station belongs to the AllSky7 fireball monitoring project and is operated by Rainer Kresken and Pablo Ramirez Moreta. We also thank all SPMN station operators whose continuous dedication have allowed to record these bolides from multiple stations: Jordi Donet Donet, Vicent Ibáñez, Jose M. Serna, Carlos Alcaraz, Antonio J. Robles, Ramón López, Agustín Núñez, José A. de los Reyes, Sensi Pastor, Antonio Fernández Sánchez, Antonio Lasala, Álex Gómez, Juan Gómez, Ramón López, Francisco José García Rodríguez and Cesar Guasch Besalduch.

DATA AVAILABILITY

The data underlying this article will be shared on reasonable request to the corresponding author.

REFERENCES

- Babadjanov P., 1963, *Smithsonian Contributions to Astrophysics*, **7**, 287
- Bagnall P. M., 2021, *Atlas of Meteor Showers; A Practical Workbook for Meteor Observers*. Springer Nature, doi:10.1007/978-3-030-76643-6
- Bannister S. M., Boucheron L. E., Voelz D. G., 2013, *PASP*, **125**, 1108
- Blum J., Schröpler R., Davidsson B. J. R., Trigo-Rodríguez J. M., 2006, *ApJ*, **652**, 1768
- Borovička J., Spurný P., Keclikova J., 1995, *A&AS*, **112**, 173
- Borovička J., 1992, *Publications of the Astronomical Institute of the Czechoslovak Academy of Sciences*, **79**
- Borovička J., Spurný P., Brown P., 2015, in *Asteroids IV*. University of Arizona Press, pp 257–280, doi:10.2458/azu_uapress_9780816532131-ch014
- Bottke William F. J., Rubincam D. P., Burns J. A., 2000, *Icarus*, **145**, 301
- Bronshten V., 1981, *Moscow, Izdatel'stvo Nauka*, 1981. 416
- Brož M., 2006, PhD thesis, Charles University in Prague
- Brown P., Spalding R. E., ReVelle D. O., Tagliaferri E., Worden S. P., 2002, *Nature*, **420**, 294
- Ceplecha Z., 1987, *Bulletin of the Astronomical Institutes of Czechoslovakia*, **38**, 222
- Ceplecha Z., Borovička J., Elford W. G., ReVelle D. O., Hawkes R. L., Porubčan V., Šimek M., 1998, *Space Sci. Rev.*, **84**, 327
- Chapman C. R., 2010, *Nature*, **463**, 305
- Chyba C. F., Thomas P. J., Zahnle K. J., 1993, *Nature*, **361**, 40
- Colas F., et al., 2020, *A&A*, **644**, A53
- Drolshagen E., et al., 2021, *A&A*, **652**, A84
- Drummond J. D., 1981, *Icarus*, **45**, 545
- Endres S. C., Sandrock C., Focke W. W., 2018, *Journal of Global Optimization*, **72**, 181
- Everhart E., 1985, in Carusi A., Valsecchi G. B., eds, *Astrophysics and Space Science Library Vol. 115, IAU Colloq. 83: Dynamics of Comets: Their Origin and Evolution*. p. 185, doi:10.1007/978-94-009-5400-7_17
- Galligan D. P., 2001, *MNRAS*, **327**, 623
- Gómez Martín J. C., Bones D. L., Carrillo-Sánchez J. D., James A. D., Trigo-Rodríguez J. M., Fegley B. J., Plane J. M. C., 2017, *ApJ*, **836**, 212
- Gritsevich M. I., 2008, *Solar System Research*, **42**, 372
- Gritsevich M. I., 2009, *Advances in Space Research*, **44**, 323
- Gritsevich M., Koschny D., 2011, *Icarus*, **212**, 877
- Gritsevich M. I., Stulov V. P., 2006, *Solar System Research*, **40**, 477
- Gritsevich M. I., Stulov V. P., Turchak L. I., 2012, *Cosmic Research*, **50**, 56
- Halliday I., 1987, *Icarus*, **69**, 550
- Halliday I., Griffin A. A., 1982, *Meteoritics*, **17**, 31
- Halliday I., Griffin A. A., Blackwell A. T., 1996, *Meteoritics & Planetary Science*, **31**, 185

- Jacchia L. G., Whipple F. L., 1961, *Smithsonian Contributions to Astrophysics*, **4**, 97
- Jenniskens P., 1994, *A&A*, **287**, 990
- Jenniskens P., 1998, *Earth, Planets and Space*, **50**, 555
- Jenniskens P., 2006, *Meteor Showers and their Parent Comets*. Cambridge University Press
- Koschny D., et al., 2019, *Space Sci. Rev.*, **215**, 34
- Kresak L., 1982, in Wilkening L. L., ed., *IAU Colloq. 61: Comet Discoveries, Statistics, and Observational Selection*. pp 56–82
- Lindblad B. A., 1971, *Smithsonian Contributions to Astrophysics*, **12**, 1
- Lyytinen E., Gritsevich M., 2016, *Planet. Space Sci.*, **120**, 35
- Madiedo J. M., Trigo-Rodríguez J. M., 2008, *Earth Moon and Planets*, **102**, 133
- Melosh H. J., 1984, *Icarus*, **59**, 234
- Murad E., Williams I. P., 2002, *Meteors in the Earth's Atmosphere*. Cambridge University Press
- Olsson-Steel D., 1986, *MNRAS*, **219**, 47
- Pauls A., Gladman B., 2005, *Meteoritics & Planetary Science*, **40**, 1241
- Peña-Asensio E., Trigo-Rodríguez J. M., Langbroek M., Rimola A., J. Robles A., 2021a, *Astrodynamics*, **5**, 347
- Peña-Asensio E., Trigo-Rodríguez J. M., Gritsevich M., Rimola A., 2021b, *MNRAS*, **504**, 4829
- Peña-Asensio E., Trigo-Rodríguez J. M., Rimola A., 2022, *AJ*, **164**, 76
- Porubčan V., Williams I. P., Kornoš L., 2004, *Earth Moon and Planets*, **95**, 697
- Rao M. S., Murthy A. G., 1974, *Australian Journal of Physics*, **27**, 679
- Rein H., Spiegel D. S., 2015, *MNRAS*, **446**, 1424
- Sansom E. K., et al., 2019, *ApJ*, **885**, 115
- Silber E. A., Boslough M., Hocking W. K., Gritsevich M., Whitaker R. W., 2018, *Advances in Space Research*, **62**, 489
- Southworth R. B., Hawkins G. S., 1963, *Smithsonian Contributions to Astrophysics*, **7**, 261
- Tamayo D., Rein H., Shi P., Hernandez D. M., 2020, *MNRAS*, **491**, 2885
- Terentjeva A. K., 1990, in Lagerkvist C. I., Rickman H., Lindblad B. A., eds, *Asteroids, Comets, Meteors III*. p. 579
- Tóth J., Vereš P., Kornoš L., 2011, *MNRAS*, **415**, 1527
- Trigo-Rodríguez J. M., 2022, *Asteroid Impact Risk: Impact Hazard from Asteroids and Comets*. Springer Nature
- Trigo-Rodríguez J. M., Blum J., 2022, *MNRAS*, **512**, 2277
- Trigo-Rodríguez J. M., Llorca J., 2006, *MNRAS*, **372**, 655
- Trigo-Rodríguez J. M., et al., 2004, *Earth Moon and Planets*, **95**, 553
- Trigo-Rodríguez J. M., Betlem H., Lyytinen E., 2005, *ApJ*, **621**, 1146
- Trigo-Rodríguez J., Madiedo J., Williams I., 2014, in Muinonen K., Penttilä A., Granvik M., Virkki A., Fedorets G., Wilkman O., Kohout T., eds, *Asteroids, Comets, Meteors 2014*. p. 533
- Trigo-Rodríguez J. M., Gritsevich M., Palme H., eds, 2017, *Dynamic Sources of Contemporary Hazard from Meteoroids and Small Asteroids Astrophysics and Space Science Proceedings Vol. 46*, doi:10.1007/978-3-319-46179-3_2.
- Trigo-Rodríguez J. M., Rimola A., Tanbakouei S., Soto V. C., Lee M., 2019, *Space Sci. Rev.*, **215**, 18
- Turchak L. I., Gritsevich M. I., 2014, *Journal of Theoretical and Applied Mechanics*, **44**, 15
- Vaubailon J., Neslušan L., Sekhar A., Rudawska R., Ryabova G. O., 2019, in Ryabova G. O., Asher D. J., Campbell-Brown M. J., eds, *Meteoroids: Sources of Meteors on Earth and Beyond*. Cambridge University Press., p. 161
- Voloshchuk Y. I., Kashcheev B. L., 1996, *Solar System Research*, **30**, 480
- Wiegert P., Brown P., 2004, *Earth Moon and Planets*, **95**, 19

This paper has been typeset from a \LaTeX file prepared by the author.